Northumbria Research Link

PROCEEDINGS A

Symmetric Waterbomb Origami

SCHOLARONE™
Manuscripts

Symmetric Waterbomb Origami

Yan Chen[1,2], Huijuan Feng[1], Jiayao Ma[1], Rui Peng[1], Zhong You[1, 3§]

[1]School of Mechanical Engineering, Tianjin University, 92 Weijin Road, Tianjin 300072, China.

[2]Key Laboratory of Mechanism Theory and Equipment Design of Ministry of Education, Tianjin University, Tianjin 300072, China

[3]Department of Engineering Science, University of Oxford, Parks Road, Oxford OX1 3PJ, UK.

[§]Corresponding author. E-mail: zhong.you@eng.ox.ac.uk, orcid.org/0000-0002-5286-7218

Abstract:

The traditional waterbomb origami, produced from a pattern consisting of a series of vertices where six creases meet, is one of the most widely utilised origami patterns. From rigid origami viewpoint, it generally has multiple degrees of freedom, but when the pattern is folded symmetrically, the mobility reduces to one. This paper presents a thorough kinematic investigation on symmetric folding of the waterbomb pattern. It has been found that the pattern can have two folding paths under certain circumstance. Moreover, the pattern can be used to fold thick panels. Not only do the additional constraints imposed to fold the thick panels lead to single degree of freedom folding, but the folding process is kinematically equivalent to the origami of zero-thickness sheets. The findings pave the way for the pattern being readily used to fold deployable structures ranging from flat roofs to large solar panels.

Keywords: Waterbomb base, waterbomb tessellation, rigid origami, thick-panel origami

Nomenclature

$z_i{}^*$	Coordinate axis of crease i or revolute joint i
x_i	Coordinate axis common normal from z_{i-1} to z_i
$\alpha_{i(i+1)}$	Angle of rotation from z_i to z_{i+1} about axis x_{i+1}, also known as the twist of link $i(i+1)$
α, β	Design angular parameters of the origami waterbomb pattern

1

$\mathbf{Q}_{i(i+1)}$ 3 by 3 transformation matrix between the coordinate system of link $(i-1)i$ and that of link $i(i+1)$ for spherical linkages

δ_i Angle of rotation from x_i to x_{i+1} about axis z_i in the vertex $\mathbf{D}$ of the origami waterbomb pattern, also known as the revolute variable of joint i

φ_i The dihedral angle between link $(i-1)i$ and link $i(i+1)$ in the vertex $\mathbf{D}$ of the origami waterbomb pattern

ω_i Angle of rotation from x_i to x_{i+1} about axis z_i in the vertex $\mathbf{W}$ of the origami waterbomb pattern, also known as the revolute variable of joint i

ϕ_i The dihedral angle between link $(i-1)i$ and link $i(i+1)$ in the vertex $\mathbf{W}$ of the origami waterbomb pattern

$a^D_{i(i+1)}$ The normal distance between z_i and z_{i+1}, also known as the link length of link $i(i+1)$ in the vertex $\mathbf{D}$ of the thick-panel waterbomb pattern or the panel thickness

$a^W_{i(i+1)}$ The normal distance between z_i and z_{i+1}, also known as the link length of link $i(i+1)$ in the vertex $\mathbf{W}$ of the thick-panel waterbomb pattern or the panel thickness

R^D_i The normal distance between x_i and x_{i+1}, also known as the offset of joint i in the vertex $\mathbf{D}$ of the thick-panel waterbomb pattern

R^W_i The normal distance between x_i and x_{i+1}, also known as the offset of joint i in the vertex $\mathbf{W}$ of the thick-panel waterbomb pattern

$\mathbf{T}_{i(i+1)}$ 4 by 4 transformation matrix between the coordinate system of link $(i-1)i$ and that of link $i(i+1)$

a Thickness parameter for thick-panel waterbomb pattern, also the thickness of link 23 in the vertex $\mathbf{W}$ of the thick-panel waterbomb pattern

μ The proportion between the thickness of link 34 and link 23 in the vertex $\mathbf{W}$ of the thick-panel waterbomb pattern

2

δ_i' Angle of rotation from x_i to x_{i+1} about axis z_i in the vertex **D** of the thick-panel waterbomb pattern, also known as the revolute variable of joint i

φ_i' The dihedral angle between link $(i-1)i$ and link $i(i+1)$ in the vertex **D** of the thick-panel waterbomb pattern

ω_i' Angle of rotation from x_i to x_{i+1} about axis z_i in the vertex **W** of the thick-panel waterbomb pattern, also known as the revolute variable of joint i

ϕ_i' The dihedral angle between link $(i-1)i$ and link $i(i+1)$ in the vertex **W** of the thick-panel waterbomb pattern

* The setup of coordinates and kinematic parameters for both zero-thickness and thick-panel origami according to Denavit–Hartenberg's (DH) notation is shown in figure A of Appendix A.

1. Introduction

The waterbomb is a traditional origami [1]. Commonly, two terms are related to it: waterbomb bases and waterbomb tessellations. There are two types of waterbomb bases: the eight-crease base and the six-crease base. The former is made from a square sheet of paper consisting of eight alternating mountain and valley creases around a central vertex, figure 1(a). One of its typical tessellations is produced by four such bases tiling around a smaller square forming the square Resch pattern, figures 1(b) and 1(c). The latter, consisting of two mountain and four valley creases shown in figure 1(d), is more commonly known, and its tessellations range from a flat-foldable surface to a deformable tube known as the magic origami ball, figures 1(e) and (f).

Both waterbomb origami structures were extensively investigated in the past. For instance, Hanna et. al. and Bowen et. al. established the bistable and dynamic model of the eight-crease waterbomb base [2, 3]. Tachi et. al. worked on the rigidity of a six-crease origami tessellation with multiple degrees of freedom to achieve an adaptive freeform surface [4]. On the application side, the first origami stent was made from the waterbomb tube aimed to achieve a large deployable ratio [5]. A worm robot [6] and a deformable wheel robot [7] were also proposed based on the magic origami ball.

3

In this paper, the focus is drawn on the six-fold waterbomb tessellation. Due to its large deployable ratio between expanded and packaged states, it can be potentially used to fold large flat roofs and space solar panels. Although the waterbomb pattern is of multiple degrees of freedom, the symmetric folding is often preferred in most of research or art work, which is done by constraining it with symmetric conditions and then controlling the motion to reach an ideal flat-foldable state. This is not easy in practice due to the fact that in rigid origami, the six-fold waterbomb base itself is a spherical $6R$ linkage with three degrees of freedom [8], thus the number of degrees of freedom for the pattern could increase significantly if the pattern consists of a large number of waterbomb bases.

The waterbomb pattern is primarily created for zero-thickness sheets just like all of the origami patterns. Yet, in most of the practical engineering applications, the thickness of the material cannot simply be ignored. Various methods have been proposed to fold thick panel. In one instance, tapered surfaces are used to fold a thick panel using the Miura-ori of zero-thickness sheet [9], whereas in the other, offsets at the edge of the panels were introduced to implement folding of thick panels using the square-twist origami pattern [10]. A more recent research suggested to replace folds with two parallel ones to accommodate the thickness of materials [11]. In all of the above methods, the fundamental kinematic model in which origami is treated as a series of interconnected spherical linkages remained. Different from the above methods, the authors of this paper have also proposed an approach in which the fold lines were only allowed to be placed on top or bottom of flat thick panels. As a result, the spherical linkage assembly for the origami of zero-thickness sheet is replaced by an assembly of spatial linkages. We have proved that not only are the assemblies of such panels foldable, but they can be folded compactly under certain conditions [12].

In this paper, we provide a comprehensive kinematic analysis on foldability of the waterbomb tessellation made from the six-fold waterbomb bases of both a zero-thickness sheet and panel of finite thickness. Kinematically the folding of zero-thickness sheet is modelled as spherical $6R$ linkages whereas that of thick panel is treated as an assembly of

4

the Bricard linkages. The analysis has revealed a number of very interesting features associated with the waterbomb origami, including the existence of two folding paths for general waterbomb origami of zero-thickness sheets when it is folded symmetrically. Moreover, because the Bricard linkages are overconstrained [14, 15], the increase in number of degrees of freedom occurring for the origami of zero-thickness sheet does not materialise for thick panels.

The paper is structured as follows. Section 2 presents a detailed analysis on rigid foldability of the waterbomb tessellation for zero-thickness sheets. This is followed by the design and kinematic behaviour of its corresponding thick-panel origami in section 3. Comparisons are made in section 4 with further discussion for potential applications.

2. Symmetric rigid folding of the waterbomb pattern of zero-thickness sheet

Consider a pattern made by tessellating six-crease waterbomb bases, figure 2(a). The pattern consists of only two types of vertices, **D** and **W**, enlarged in figures 2(b) and 2(c). The rigid origami folding around each vertex can be modelled kinematically as a spherical $6R$ linkage in which the creases act as revolute joints and the sheets between creases are rigid links. In general, a spherical $6R$ linkage is of three degrees of freedom, but this number is reduced to one if only the symmetric folding is allowed. In such a way, vertex **D** is regarded as a spherical $6R$ linkage with the geometric parameters $\alpha_{12} = \alpha_{34} = \alpha_{45} = \alpha_{61} = \alpha$, $\alpha_{23} = \alpha_{56} = \pi - 2\alpha$, where $0 < \alpha \le \dfrac{\pi}{2}$. Imposing the line and plane symmetry conditions, i.e., $\delta_1 = \delta_4$ and $\delta_2 = \delta_3 = \delta_5 = \delta_6$, to the closure condition of the linkage (see Appendix A), we can then write the closure equations as

$$\tan\frac{\delta_1}{2} = -\cos\alpha\tan\frac{\delta_2}{2}, \text{ and } \delta_1 = \delta_4, \ \delta_2 = \delta_3 = \delta_5 = \delta_6. \tag{1}$$

Similarly applying the symmetry condition to vertex **W**, it becomes a plane-symmetric spherical $6R$ linkage with the geometric parameters $\alpha_{12} = \alpha_{61} = \pi - \alpha - \beta$, $\alpha_{23} = \alpha_{56} = \beta$, $\alpha_{34} = \alpha_{45} = \alpha$, where $0 < \beta \le \dfrac{\pi}{2}$, and

$$\omega_5 = \omega_3, \ \omega_6 = \omega_2. \tag{2a}$$

5

To ensure the compatibility of the entire pattern, the kinematic relationship between ω_1 and ω_3 of vertex **W** must be identical to that between δ_1 and δ_2 of vertex **D**. Replacing δ_1 and δ_2 in equation (1) with ω_1 and ω_3, respectively, yields

$$\tan\frac{\omega_1}{2} = -\cos\alpha\tan\frac{\omega_3}{2}. \tag{2b}$$

Now considering the closure condition of the linkage at **W**, we obtain two sets of equations. The first set is

$$\tan\frac{\omega_2}{2} = -\frac{\cos\alpha}{\cos(\alpha+\beta)}\tan\frac{\omega_3}{2}, \tag{3a}$$

$$\omega_4 = \omega_1, \tag{3b}$$

whilst the second one is

$$\tan\frac{\omega_2}{2} = -\frac{2\sin\alpha\tan\dfrac{\omega_3}{2}}{\sin(\beta-\alpha)\tan^2\dfrac{\omega_3}{2}+\sin(\alpha+\beta)}, \tag{4a}$$

and

$$\tan\frac{\omega_4}{2} = \frac{\tan\dfrac{\omega_3}{2}\left(-2\cos\alpha\sin^2(\beta-\alpha)\tan^4\dfrac{\omega_3}{2}+4(\sin\alpha\sin 2\beta+\cos\alpha\sin(\alpha+\beta)\sin(\beta-\alpha))\tan^2\dfrac{\omega_3}{2}\right.}{2\sin(\beta-\alpha)(2\sin(\alpha+\beta)+\sin(\beta-\alpha))\tan^4\dfrac{\omega_3}{2}+4(\cos^2(\alpha+\beta)-\cos 2\beta)\tan^2\dfrac{\omega_3}{2}-2\sin^2(\alpha+\beta)}.$$

$$\left.\frac{+\sin(\alpha+\beta)(7\sin\beta-\sin(2\alpha+\beta)))}{}\right. \tag{4b}$$

Together with equations (1) and (2), the entire sets of closure equations of waterbomb pattern have been obtained.

The kinematic variables, or rotations about each crease, can be replaced by the dihedral angles between adjacent sheets connected by the crease. The relationship between the kinematic variables and dihedral angels are $\delta_1 = \pi - \varphi_1$, $\delta_2 = \pi + \varphi_2$, $\delta_3 = \pi + \varphi_3$, $\delta_4 = \pi - \varphi_4$, $\delta_5 = \pi + \varphi_5$, $\delta_6 = \pi + \varphi_6$ for vertex **D** and $\omega_1 = \pi - \phi_1$, $\omega_2 = \pi - \phi_2$, $\omega_3 = \pi + \phi_3$, $\omega_4 = \pi - \phi_4$, $\omega_5 = \pi + \phi_5$, $\omega_6 = \pi - \phi_6$ for vertex **W**. Thus the two sets of

6

kinematic relationships of the waterbomb pattern presented by the dihedral angels become

$$\tan\frac{\phi_1}{2} = \frac{1}{\cos\alpha}\tan\frac{\phi_3}{2}, \tag{5a}$$

$$\tan\frac{\phi_2}{2} = \frac{\cos(\alpha+\beta)}{\cos\alpha}\tan\frac{\phi_3}{2}, \tag{5b}$$

$$\phi_4 = \phi_1,\ \phi_5 = \phi_3,\ \phi_6 = \phi_2, \tag{5c}$$

$$\varphi_2 = \phi_3, \tag{5d}$$

$$\tan\frac{\varphi_1}{2} = \frac{1}{\cos\alpha}\tan\frac{\varphi_2}{2},\ \varphi_1 = \varphi_4,\ \varphi_2 = \varphi_3 = \varphi_5 = \varphi_6; \tag{5e}$$

and

$$\tan\frac{\phi_1}{2} = \frac{1}{\cos\alpha}\tan\frac{\phi_3}{2}, \tag{6a}$$

$$\tan\frac{\phi_2}{2} = \frac{\sin(\alpha+\beta)\tan^2\dfrac{\phi_3}{2} + \sin(\beta-\alpha)}{2\sin\alpha\tan\dfrac{\phi_3}{2}}, \tag{6b}$$

$$\tan\frac{\phi_4}{2} = \frac{\begin{array}{c}\tan\dfrac{\phi_3}{2}\left(2\sin^2(\alpha+\beta)\tan^4\dfrac{\phi_3}{2} - 4(\cos^2(\alpha+\beta)-\cos 2\beta)\tan^2\dfrac{\phi_3}{2}\right.\\[6pt] \left.-2\sin(\beta-\alpha)(2\sin(\alpha+\beta)+\sin(\beta-\alpha))\right)\end{array}}{\begin{array}{c}\sin(\alpha+\beta)(7\sin\beta - \sin(2\alpha+\beta))\tan^4\dfrac{\phi_3}{2}\\[6pt] +4(\sin\alpha\sin 2\beta + \cos\alpha\sin(\alpha+\beta)\sin(\beta-\alpha))\tan^2\dfrac{\phi_3}{2} - 2\cos\alpha\sin^2(\beta-\alpha)\end{array}}, \tag{6c}$$

$$\phi_5 = \phi_3,\ \phi_6 = \phi_2, \tag{6d}$$

$$\varphi_2 = \phi_3, \tag{6e}$$

$$\tan\frac{\varphi_1}{2} = \frac{1}{\cos\alpha}\tan\frac{\varphi_2}{2},\ \varphi_1 = \varphi_4,\ \varphi_2 = \varphi_3 = \varphi_5 = \varphi_6. \tag{6f}$$

Considering a pattern with $\alpha = \dfrac{2\pi}{9}$, $\beta = \dfrac{2\pi}{9}$, and taking ϕ_1 as an input, the variations of other dihedral angles at vertex **W** with respect to ϕ_1 are plotted in figure 3(a). There are two paths with the same starting point (π, π) and ending point $(0, 0)$: *Path I* based on

7

equations (5a-e) and *Path II* on equations (6a-f). It indicates that vertex **W** can be folded compactly along two different paths. Yet for vertex **D**, with $\varphi_1 = \varphi_4 = \phi_1$, there is only one path, see figure 3(b). Therefore, in general the patterns with a large number of vertices **D** and **W** will fold in two different manners, from i, ii, iii, iv to v, or from i, viii, vii, vi to v, as demonstrated in figure 3(c).

There are a few special cases of the waterbomb pattern which are mostly interesting. First, when $\alpha + \beta = \pi/2$, creases along z_2 and z_6 at vertex **W** shown in figure 2(c) become collinear. As a result, they fold together like a single crease. *Path I*, given by equation (5), breaks down into two straight lines. A particular case with $\alpha = \beta = \dfrac{\pi}{4}$ is shown in figure 4. At the first folding stage, ϕ_2 (and ϕ_6) starts from π and finishes at 0 from i, xi, x and ix, while ϕ_1, ϕ_3, ϕ_4, and ϕ_5 remain to be π, then ϕ_2 (and ϕ_6) is kept at constant 0 and ϕ_1, ϕ_3, ϕ_4, and ϕ_5 changes from π to 0 along ix, viii, vii, vi and v. Both reach the compactly folded configuration. At the latter stage, vertex **W** behaves like a spherical 4*R* linkage because ϕ_2 and ϕ_6 are frozen. The movement around vertex **W** will drive vertex **D** to move accordingly.

Second, equations (5) or (6) could give negative dihedral angles, which indicates blockage occurring during folding because physically the dihedral angles cannot be less than zero. By analysing equation (5b), it can be found that for *Path I* when $\alpha + \beta > \dfrac{\pi}{2}$, ϕ_2 is always negative except at points $(0, 0)$ and (π, π). So blockage is always there. And from equation (6c), it can be found that on *Path II* when $\alpha \neq \beta$, blockage will occur when

$$\frac{1}{\cos\alpha}\sqrt{\frac{-2\left(\begin{array}{c}\sin\alpha\sin 2\beta \\ +\cos\alpha\sin(\alpha+\beta)\sin(\beta-\alpha)\end{array}\right)+\sqrt{\begin{array}{c}4(\sin\alpha\sin 2\beta+\cos\alpha\sin(\alpha+\beta)\sin(\beta-\alpha))^2 \\ +2\cos\alpha\sin^2(\beta-\alpha)\sin(\alpha+\beta)(7\sin\beta-\sin(2\alpha+\beta))\end{array}}}{\sin(\alpha+\beta)(7\sin\beta-\sin(2\alpha+\beta))}}$$

$$< \tan\frac{\phi_1}{2} < \frac{\sqrt{\cos^2(\alpha+\beta)-\cos 2\beta+\sqrt{\begin{array}{c}(\cos^2(\alpha+\beta)-\cos 2\beta)^2 \\ +\sin(\beta-\alpha)\sin^2(\alpha+\beta)(2\sin(\alpha+\beta)+\sin(\beta-\alpha))\end{array}}}}{\cos\alpha\sin(\alpha+\beta)}$$

$$(7)$$

For example, when $\alpha = \frac{7\pi}{36}$, $\beta = \frac{\pi}{4}$, the kinematic curve between ϕ_4 and ϕ_1 is shown in figure 5(a) and the folding sequences are demonstrated in figure 5(b). Along *Path I*, the pattern can be folded from a sheet at i to fully folded configuration at vii, whereas along *Path II*, the folding process terminates at iii. The framed configurations are physically impossible due to blockage because these configurations correspond to cases where ϕ_4 becomes negative. Even if the penetrations were allowed, the folding along *Path II* would end up in a fully folded configuration at vi that differs from that at vii along *Path I*.

The physical blockage can also occur when $\alpha + \beta = \frac{\pi}{2}$ but $\alpha \neq \beta$. Figure 5(c) shows a two-stage motion on *Path I* and blockage on *Path II* for a pattern with $\alpha = \frac{\pi}{6}$ and $\beta = \frac{\pi}{3}$. Based on the above analysis, the behaviour of the waterbomb tessellation can be summarized as follows.

(a) When $\alpha + \beta < \frac{\pi}{2}$ and $\alpha = \beta$, there are two smooth folding paths without either two-stage motion or blockage.

(b) When $\alpha + \beta < \frac{\pi}{2}$ and $\alpha \neq \beta$, *Path II* is blocked and *Path I* is smooth;

(c) When $\alpha + \beta = \frac{\pi}{2}$ and $\alpha = \beta$, *Path I* is in two-stage motion while *Path II* is smooth;

(d) When $\alpha + \beta = \frac{\pi}{2}$ and $\alpha \neq \beta$, both two-stage motion on *Path I* and blockage on *Path II* happen.

9

(e) When $\alpha + \beta > \dfrac{\pi}{2}$ and $\alpha = \beta$, only *Path II* for vertex **W** is smooth, but vertex **D** is

blocked. Thus the whole pattern is blocked from compact folding; and

(f) When $\alpha + \beta > \dfrac{\pi}{2}$ but $\alpha \neq \beta$, both paths are blocked.

Among them, only cases (a) – (c) can have one or two smooth folding paths.

3. Folding thick panels with the waterbomb pattern

The waterbomb tessellation can also be used to fold panels with non-zero thickness. This is done by mapping the same pattern onto a thick panel while placing the fold lines either on top or bottom surfaces of the panel. Now at **D** and **W**, there will still be six fold lines in places of creases, but these fold lines no longer converge to a vertex. In other words, dissimilar to zero-thickness sheet, the distances between the adjacent fold lines are no longer zeros. In terms of kinematic model, the spherical $6R$ linkage is now replaced by spatial $6R$ linkages. Among all possible spatial $6R$ linkages, the plane-symmetric Bricard linkage [16], is the most suitable one [12]. Let us select two Bricard linkages for **D** and **W**, respectively, figures 6(a) and (b), with their link lengths being the panel thicknesses. As the linkages are overconstrained, the geometric conditions of the linkage at **D** are

$$a_{12}^D = a_{61}^D = a_{34}^D = a_{45}^D = (2 + \mu)a, \; a_{23}^D = a_{56}^D = 0, \tag{8a}$$

$$\alpha_{12}^D = 2\pi - \alpha, \; \alpha_{61}^D = \alpha, \; \alpha_{23}^D = \pi - 2\alpha, \; \alpha_{56}^D = \pi + 2\alpha, \; \alpha_{34}^D = \alpha, \; \alpha_{45}^D = 2\pi - \alpha, \tag{8b}$$

$$R_i^D = 0 \; (i = 1, 2, 3, 4, 5, 6); \tag{8c}$$

and those at **W** are

$$a_{12}^W = a_{61}^W = (1 + \mu)a, \; a_{23}^W = a_{56}^W = a, \; a_{34}^W = a_{45}^W = \mu a, \tag{9a}$$

$$\alpha_{12}^W = \pi - \alpha - \beta, \; \alpha_{61}^W = \pi + \alpha + \beta, \; \alpha_{23}^W = \beta, \; \alpha_{56}^W = 2\pi - \beta, \; \alpha_{34}^W = 2\pi - \alpha, \; \alpha_{45}^W = \alpha, \tag{9b}$$

$$R_i^W = 0 \; (i = 1, 2, 3, 4, 5, 6), \tag{9c}$$

Here, α and β are the same as the sector angles of the origami pattern in figures 2(b) and (c) and α_{ij}^D and α_{ij}^W are expressed using the DH notation [16], while a is the thickness of link 23 and μ is the proportion between the thickness of link 34 and link 23 in the vertex **W** of the thick-panel waterbomb pattern where $a \neq 0$ and $\mu \neq 0$.

10

Applying the closure condition of the linkages leads to the following closure equations (see Appendix A). For **D**, two sets of closure equations can be obtained, which are

$$\tan\frac{\delta_1'}{2} = -\frac{1}{\cos\alpha}\tan\frac{\delta_2'}{2}, \ \delta_3' = \delta_2' + \pi, \ \delta_4' = \delta_1', \ \delta_5' = \delta_3', \ \delta_6' = \delta_2'; \tag{10}$$

and

$$\tan\frac{\delta_1'}{2} = \frac{2\cos\alpha\tan\dfrac{\delta_2'}{2}}{\tan^2\dfrac{\delta_2'}{2} - \cos 2\alpha}, \ \delta_3' = \pi - \delta_2', \ \delta_4' = -\delta_1', \ \delta_5' = \delta_3', \ \delta_6' = \delta_2', \tag{11}$$

respectively. The relationship between the kinematic variables and dihedral angels at **D** are $\delta_1' = 2\pi - \varphi_1'$, $\delta_2' = \varphi_2'$, $\delta_3' = \pi + \varphi_3'$, $\delta_4' = 2\pi - \varphi_4'$, $\delta_5' = \pi + \varphi_5'$, $\delta_6' = \varphi_6'$. By conversion of the kinematic variables to the dihedral angels, the two sets of closure equations can be respectively rewritten as

$$\tan\frac{\varphi_1'}{2} = \frac{1}{\cos\alpha}\tan\frac{\varphi_2'}{2}, \tag{12a}$$

$$\varphi_4' = \varphi_1', \ \varphi_2' = \varphi_3' = \varphi_5' = \varphi_6'; \tag{12b}$$

and

$$\tan\frac{\varphi_1'}{2} = \frac{2\cos\alpha\tan\dfrac{\varphi_2'}{2}}{-\tan^2\dfrac{\varphi_2'}{2} + \cos 2\alpha}, \tag{13a}$$

$$\varphi_3' = -\varphi_2', \ \varphi_4' = -\varphi_1', \ \varphi_5' = \varphi_3', \ \varphi_6' = \varphi_2', \tag{13b}$$

Similarly, we also have two sets of closure equations at **W**, which are

$$\tan\frac{\omega_1'}{2} = -\frac{1}{\cos\alpha}\tan\frac{\omega_3'}{2}, \tag{14a}$$

$$\tan\frac{\omega_2'}{2} = \frac{\cos\alpha}{\cos(\alpha+\beta)}/\tan\frac{\omega_3'}{2}, \tag{14b}$$

$$\omega_4' = \omega_1', \ \omega_5' = \omega_3', \ \omega_6' = \omega_2'; \tag{14c}$$

and

11

$$\tan\frac{\omega_1'}{2} = \frac{-\tan\frac{\omega_3'}{2}(\mu\sin^2(\alpha+\beta)\tan^2\frac{\omega_3'}{2} + (\mu+1)(\mu\sin^2\beta + \sin^2\alpha))}{\sin(\alpha+\beta)(\mu^2\sin\beta + \cos(\alpha+\beta)\sin\alpha)\tan^2\frac{\omega_3'}{2} + (\mu+1)^2\sin\alpha\sin\beta\cos\beta}, \quad (15a)$$

$$\tan\frac{\omega_2'}{2} = \frac{(\mu+1)\sin\alpha}{\mu\sin(\alpha+\beta)} / \tan\frac{\omega_3'}{2}, \quad (15b)$$

$$\tan\frac{\omega_4'}{2} = \frac{-\tan\frac{\omega_3'}{2}(4\mu\sin\alpha\sin^2(\alpha+\beta)\tan^2\frac{\omega_3'}{2} - 4(\mu+1)\sin\alpha((\mu+1)\sin^2\beta - \sin^2(\alpha+\beta)))}{(\cos(3\alpha+\beta) - 2(1+\mu)^2\cos(\alpha+\beta) + (1+4\mu+2\mu^2)\cos(\alpha-\beta))\sin(\alpha+\beta)\tan^2\frac{\omega_3'}{2} + 2(\mu+1)^2\sin^2\alpha\sin 2\beta}$$

$$(15c)$$

$$\omega_5' = \omega_3', \; \omega_6' = \omega_2'. \quad (15d)$$

The above two sets of closure equations can be written in terms of dihedral angles. Noting that the relationship between the kinematic variables and dihedral angles at **W** are $\omega_1' = 2\pi - \phi_1'$, $\omega_2' = \pi - \phi_2'$, $\omega_3' = \phi_3'$, $\omega_4' = 2\pi - \phi_4'$, $\omega_5' = \phi_5'$, $\omega_6' = \pi - \phi_6'$, the two sets of closure equations now become

$$\tan\frac{\phi_1'}{2} = \frac{1}{\cos\alpha}\tan\frac{\phi_3'}{2}, \quad (16a)$$

$$\tan\frac{\phi_2'}{2} = \frac{\cos(\alpha+\beta)}{\cos\alpha}\tan\frac{\phi_3'}{2}, \quad (16b)$$

$$\phi_4' = \phi_1', \; \phi_5' = \phi_3', \; \phi_6' = \phi_2'; \quad (16c)$$

and

$$\tan\frac{\phi_1'}{2} = \frac{\tan\frac{\phi_3'}{2}(\mu\sin^2(\alpha+\beta)\tan^2\frac{\phi_3'}{2} + (\mu+1)(\mu\sin^2\beta + \sin^2\alpha))}{\sin(\alpha+\beta)(\mu^2\sin\beta + \cos(\alpha+\beta)\sin\alpha)\tan^2\frac{\phi_3'}{2} + (\mu+1)^2\sin\alpha\sin\beta\cos\beta}, \quad (17a)$$

$$\tan\frac{\phi_2'}{2} = \frac{\mu\sin(\alpha+\beta)}{(\mu+1)\sin\alpha}\tan\frac{\phi_3'}{2}, \quad (17b)$$

12

$$\tan\frac{\phi_4'}{2} = \frac{\tan\frac{\phi_3'}{2}\left(4\mu\sin\alpha\sin^2(\alpha+\beta)\tan^2\frac{\phi_3'}{2} - 4(\mu+1)\sin\alpha\left((\mu+1)\sin^2\beta - \sin^2(\alpha+\beta)\right)\right)}{\left(\cos(3\alpha+\beta) - 2(1+\mu)^2\cos(\alpha+\beta) + (1+4\mu+2\mu^2)\cos(\alpha-\beta)\right)\sin(\alpha+\beta)\tan^2\frac{\phi_3'}{2} + 2(\mu+1)^2\sin^2\alpha\sin2\beta}$$

(17c)

$$\phi_5' = \phi_3', \ \phi_6' = \phi_2'.$$

(17d)

So far, two complete sets of closure equations have been obtained. It can be noted from all closure equations that the motions of the linkages retain the plane symmetry. Additional compatibility conditions between the vertices **D** and **W** need to be added, which are

$$\phi_1' = \varphi_1' \text{ and } \phi_3' = \varphi_2'.$$

(18)

We shall now discuss the respective motion paths provided by two sets of closure equations.

- The first set of closure equations, equation (12), at **D** and the first set of closure equations, equation (16) at **W**

Because equations (12a) and (16a) are identical, the compatibility between **D** and **W**, equation (18), is satisfied automatically. Therefore, there is always a smooth folding path for the thick-panel origami for any $\mu \neq 0$, figure 7(a-c), in which μ is randomly selected as 0.5. By comparing equations (12) and (16) for the thick panel with equations (5) for the zero-thickness sheet, we can conclude that the thick-panel origami and the *Path I* of the original waterbomb origami pattern are kinematically identical, as demonstrated by the folding sequence of the physical models in figure 7(d). The motions of both structures are line and plane symmetric. Moreover, when $\alpha + \beta = \frac{\pi}{2}$, *Path I* becomes a two-stage motion, where ϕ_2' and ϕ_6' changing from π to 0 while ϕ_1', ϕ_3', ϕ_4', and ϕ_5' kept to π, followed by the process that ϕ_1', ϕ_3', ϕ_4', and ϕ_5' move as a spatial 4R linkage. This linkage is actually a Bennett linkage. And it eventually reaches the compact folding

13

position. However, blockage could be occurred during the motion due to the panel thickness, which makes the structure cannot be fully folded, see figure 8, in which μ is randomly selected as 0.7.

• The first set of closure equations, equation (12), at **D** and the second set of closure equations, equation (17) at **W**

Consider equations (12a) and (17a). Under the compatibility condition given by equation (18), there must be

$$\mu = \frac{\cos(\alpha + \beta)\sin\alpha}{\sin\beta} \tag{19a}$$

Additionally when $\alpha = \beta$, another solution exists, which is

$$\mu = 1. \tag{19b}$$

Under the first solution given in (19a), equation (17) effectively coincides with equation (16), and thus there is only one set of closure equations for **W**. Only one folding path exists as shown in figure 9 for the case where $\alpha = \frac{7\pi}{36}$, $\beta = \frac{\pi}{4}$ and $\mu = 0.14$. Note that this path matches that shown in figure 7(c) despite that in the latter, μ is randomly selected as 0.5. The motion behaviour of the thick-panel waterbomb remains the same as the zero-thickness origami in *Path I*, and thus we name it *Path I* for thick panel origami. Moreover, when $\alpha + \beta = \frac{\pi}{2}$, $\mu = 0$ from equation (19a). So it will not be considered.

Under the second solution, $\mu = 1$, given by (19b), equations (16) and (17) are different. In other words, together with equation (12), there are two sets of closure equations for the thick-panel origami with $\mu = 1$ that result in two folding paths. The first, based on equations (12) and (16), has been discussed earlier. The second, based on equations (12) and (17), are actually identical to equation (6) of the zero-thickness sheet. This shows that the corresponding folding path is kinematically identical to the *Path II* of the waterbomb origami pattern of the zero-thickness sheet, and thus it is named as *Path II* of the thick panel origami. One of such example is shown in figure 10.

14

In thick panel origami, there is also blockage because of collision of panels during the folding process. Generally along *Path I* of **W**, the blockage would appear when one of the dihedral angles becomes negative. The condition without blockage is $\phi_2' > 0$. Considering equation (16b) leads to $\alpha + \beta < \pi/2$, which is the same conclusion as zero-thickness origami pattern summarized in last section. And to avoid the interference at **D** during the folding, $0 < \alpha \le \dfrac{\pi}{4}$ must be satisfied.

- The second set of closure equations, equation (13), at **D**

The other set of closure equations given by equation (13) at **D** signify that in the thick-panel case, there exists a folding path that violates the line-symmetry. However, this path is practically always blocked since φ_3' and φ_2', φ_4' and φ_1' always have opposite signs as indicated by equation (13b).

Therefore, the behaviour of the general thick-panel waterbomb can be summarized as follows.

(a) For any $\mu \ne 0$, when $\alpha + \beta < \dfrac{\pi}{2}$, there is only one smooth folding path: *Path I*.

(b) For any $\mu \ne 0$, when $\alpha + \beta = \dfrac{\pi}{2}$, there is one two-stage folding path, *Path I*, with blockage.

(c) For any $\mu \ne 0$, when $\alpha + \beta > \dfrac{\pi}{2}$, there is one blocked folding path.

In particular,

(d) For $\mu = 1$, when $\alpha + \beta < \dfrac{\pi}{2}$, $\alpha = \beta$, there are two smooth folding paths, kinematically equivalent to *Paths I* and *II* in the zero-thickness origami.

15

(e) For $\mu = 1$, when $\alpha = \beta = \dfrac{\pi}{4}$, *Path I* is in two-stage motion and blocked, but *Path II* can achieve smooth folding.

Here, *Paths I* and *II* cannot be switch from one to another once the motions are underway. The choice of folding paths has to be made at the start and end configurations. The detailed comparison on the kinematic behaviour of the general waterbomb tessellation of zero-thickness sheets and thick panels for different design parameters is given in table B of Appendix B.

4. Conclusions and discussion

In this paper, we have analysed the rigid origami of the waterbomb tessellation of both zero-thickness sheets and thick panels under the symmetric motion condition. By introducing the plane-symmetric Bricard linkages to replace the spherical $6R$ linkages in the origami pattern, the thick-panel waterbomb structure has been successfully formed. The rigorous enforcement of compatibility conditions ensures the mobility and flat-foldability of the thick-panel origami. We have also proven that the thick-panel origami and that of the zero-thickness sheet are kinematically equivalent.

Despite the fact that the thick panel origami is born from an existing origami of zero-thickness sheet, it has a number of advantages over its parent. First, kinematically the thick-panel origami structure is a mobile assembly of overconstrained Bricard linkages with only one degree of freedom, and thus no additional constraints are required to keep its motion symmetrical. This could be a great benefit for real engineering applications as its control system could become much more simple and reliable. Second, in general, the origami of waterbomb tessellation for zero-thickness sheet has kinematic singularity when it is flat and fully compact. However, for thick panel origami, the singularity only appears when a very specific thickness is chosen. A suitable selection of the thickness of the panels make the latter possible to achieve compact folding without bifurcations. The unique motion path is certainly much desirable for most practical applications.

16

The waterbomb tessellation for the thick panels enables the structure to be folded compactly. The compactness of the package depends on the thickness coefficient and the number of vertices within the pattern. The pattern can be divided into strips formed by vertices **D** in the horizontal direction. Consider a pattern consisting of m strips, each with n vertices **D**. In the completely packaged configuration, the dimension in the vertical direction will be $(m+1)/2$ of the height of the larger triangles in the vertex **D** and the cross-section dimensions are the width of the larger triangles in the vertex **D** and the overall thickness as $2n(2+2\mu)a$, where n is the number of vertices **D** in the strip and $\mu \leq 1$. $\mu > 1$ is not recommended because it results in panels with considerable thickness and in turn, the overall thickness of the package when the panels are packaged. So the ratio between the area of a fully expanded shape and that of completely folded is about $4n$. This indicates that the concept is very suitable to fold a structure in a long rectangular shape. On the other hand, to meet the geometrical conditions of the spatial linkages, each panel within the pattern could not be of the same thickness. As a result, the overall structure in the fully deployed configuration is flat but not absolutely even. However, for this waterbomb pattern, we have manage to make sure that one side of the expanded surface is completely flat, which enables the waterbomb origami pattern to be directly applicable to fold thick-panel structures such as solar panels and space mirrors.

• **Data accessibility**

This work does not have any experimental data.

• **Competing interests**

We have no competing interests.

• **Authors' contributions:**

YC and ZY initiated the project, worked on this topic and wrote the paper. HF conducted all the equation derivation under the supervision of YC and JM. RP constructed all the models. JM did all the verification between the analytical and modelling results. All authors gave final approval for publication.

17

• **Ethics statement:**

This research poses no ethical considerations.

18

123456789101112131415161718192021222324252627282930313233343536373839404142434445464748495051525354555657585960

References

[1] http://www.britishorigami.info/academic/lister/waterbomb.php

[2] Hanna B H, Lund J M, Lang R J, Magleby S P, and Howell L L, 2014, Waterbomb Base: A Symmetric Single-Vertex Bistable Origami Mechanism, *Smart Materials and Structures*, 23(9), pp. 094009.

[3] Bowen L, Springsteen K, Feldstein H, Frecker M, Simpson T W, and Lockette P V, 2015, Development and Validation of a Dynamic Model of Magneto-Active Elastomer Actuation of the Origami Waterbomb Base, *Journal of Mechanisms and Robotics*, 7(1), pp. 011010.

[4] Tachi T, Masubuchi M, and Iwamoto M, 2011, Rigid Origami Structures with Vacuumatics: Geometric Considerations, *Proceedings of the IASS-APCS Seoul, Korea*.

[5] Kuribayashi K, Tsuchiya K, You Z, Tomus D, Umemoto M, Ito T, and Sasaki M, 2006, Self-Deployable Origami Stent Grafts as a Biomedical Application of Ni-Rich Tini Shape Memory Alloy Foil, *Materials Science and Engineering: A*, 419(1-2), pp. 131-137.

[6] Onal C D, Wood R J, and Rus D, 2013, An Origami-Inspired Approach to Worm Robots, *Mechatronics, IEEE/ASME Transactions on*, 18(2), pp. 430-438.

[7] Lee D-Y, Kim J-S, Kim S-R, Koh J-S, and Cho K-J, 2013, The Deformable Wheel Robot Using Magic-Ball Origami Structure, *ASME 2013 International Design Engineering Technical Conferences & Computers and Information in Engineering Conference IDETC/CIE 2013*, Portland, Oregon, USA.

[8] Chiang C H, *Kinematics of Spherical Mechanisms*, Krieger Pub. Co., 2000.

[9] Tachi T, Rigid-foldable thick origami. In Origami[5], AK Peters, 253-264 (2011).

[10] Edmondson B J, et al., An offset panel technique for thick rigidily foldable origami. *ASME 2014 International Design Engineering Technical Conferences*, Buffalo, NY, 17-21 Aug 2014.

[11] Ku J S and Demaine E D, Folding flat crease patterns with thick materials, *Journal of Mechanisms and Robotics*, JMP-15-1159, doi:10.1115/1.4031954 (2015).

[12] Chen Y, Peng R and You Z, Origami of thick panels, *Science*, 349, 396 (2015).

19

[13] Phillips J, *Freedom of Machinery, Volumes II*, (Cambridge Univ. Press, Cambridge, 1990).

[14] You Z, Chen Y, *Motion Structures*, (Spon press, 2012).

[15] Bricard R, Leçons de cinématique, *Tome II Cinématique Appliquée*, Gauthier-Villars, Paris, 7-12 (1927).

[16] Beggs J S, *Advanced Mechanism*, (Macmillan Company, New York, 1966).

Appendix A

According to the DH notation set up in figure A, the transformation matrix can be assembled as

$$\mathbf{T}_{(i+1)i} = \begin{bmatrix} \cos\theta_i & -\cos\alpha_{i(i+1)}\sin\theta_i & \sin\alpha_{i(i+1)}\sin\theta_i & a_{i(i+1)}\cos\theta_i \\ \sin\theta_i & \cos\alpha_{i(i+1)}\cos\theta_i & -\sin\alpha_{i(i+1)}\cos\theta_i & a_{i(i+1)}\sin\theta_i \\ 0 & \sin\alpha_{i(i+1)} & \cos\alpha_{i(i+1)} & R_i \\ 0 & 0 & 0 & 1 \end{bmatrix}, \tag{A1}$$

which transforms the expression in the $i+1$ th coordinate system to the i th coordinate system. And the inverse transformation can be expressed as

$$\mathbf{T}_{i(i+1)} = \begin{bmatrix} \cos\theta_i & \sin\theta_i & 0 & -a_{i(i+1)} \\ -\cos\alpha_{i(i+1)}\sin\theta_i & \cos\alpha_{i(i+1)}\cos\theta_i & \sin\alpha_{i(i+1)} & -R_i\sin\alpha_{i(i+1)} \\ \sin\alpha_{i(i+1)}\sin\theta_i & -\sin\alpha_{i(i+1)}\cos\theta_i & \cos\alpha_{i(i+1)} & -R_i\cos\alpha_{i(i+1)} \\ 0 & 0 & 0 & 1 \end{bmatrix}. \tag{A2}$$

For a single loop linkage consisting of six links, the closure equation is

$$\mathbf{T}_{21} \cdot \mathbf{T}_{32} \cdot \mathbf{T}_{43} = \mathbf{T}_{61} \cdot \mathbf{T}_{56} \cdot \mathbf{T}_{45}. \tag{A3}$$

As for spherical linkages, the axes intersect at one point, which means the lengths of each links are zeros and thus equation (A3) reduces to

$$\mathbf{Q}_{21} \cdot \mathbf{Q}_{32} \cdot \mathbf{Q}_{43} = \mathbf{Q}_{61} \cdot \mathbf{Q}_{56} \cdot \mathbf{Q}_{45}, \tag{A4}$$

where

$$\mathbf{Q}_{(i+1)i} = \begin{bmatrix} \cos\theta_i & -\cos\alpha_{i(i+1)}\sin\theta_i & \sin\alpha_{i(i+1)}\sin\theta_i \\ \sin\theta_i & \cos\alpha_{i(i+1)}\cos\theta_i & -\sin\alpha_{i(i+1)}\cos\theta_i \\ 0 & \sin\alpha_{i(i+1)} & \cos\alpha_{i(i+1)} \end{bmatrix}, \tag{A5}$$

and the inverse transformation is

$$\mathbf{Q}_{i(i+1)} = \begin{bmatrix} \cos\theta_i & \sin\theta_i & 0 \\ -\cos\alpha_{i(i+1)}\sin\theta_i & \cos\alpha_{i(i+1)}\cos\theta_i & \sin\alpha_{i(i+1)} \\ \sin\alpha_{i(i+1)}\sin\theta_i & -\sin\alpha_{i(i+1)}\cos\theta_i & \cos\alpha_{i(i+1)} \end{bmatrix}. \tag{A6}$$

Equations (A3) and (A4) can be used to obtain the closure equations of the thick-panel waterbomb pattern and the original waterbomb origami pattern in the text, respectively.

21

Appendix B

Table B. Kinematic behaviour of the general waterbomb tessellation of zero-thickness sheets and thick panels

| Geometric conditions		Folding paths	The waterbomb tessellation of zero-thickness sheets	The waterbomb tessellation of thick panels
$\alpha + \beta < \dfrac{\pi}{2}$	$\alpha = \beta$	*Path I*	smooth	smooth
		Path II	smooth	exists only when $\mu = 1$ and the path is smooth
	$\alpha \neq \beta$	*Path I*	smooth	smooth
		Path II	blocked	non-existent
$\alpha + \beta = \dfrac{\pi}{2}$	$\alpha = \beta$	*Path I*	two-stage motion	two-stage motion and blocked
		Path II	smooth	exists only when $\mu = 1$ and the path is smooth
	$\alpha \neq \beta$	*Path I*	two-stage motion	two-stage motion and blocked
		Path II	blocked	non-existent
$\alpha + \beta > \dfrac{\pi}{2}$	$\alpha = \beta$	*Path I*	blocked	blocked
		Path II	blocked while the path for vertex **W** is smooth	exists only when $\mu = 1$ but the path is blocked
	$\alpha \neq \beta$	*Path I*	blocked	blocked
		Path II	blocked	non-existent

22

Captions of figures

Figure 1   Two waterbomb bases and their tessellations. (a) The eight-fold waterbomb base; (b) one of its tessellations forming the Resch pattern; (c) partially folded Resch pattern model; (d) the six-fold waterbomb base; (e) its tessellation in unfolded and folded states; and (f) the tessellation can also be used to form a tube.
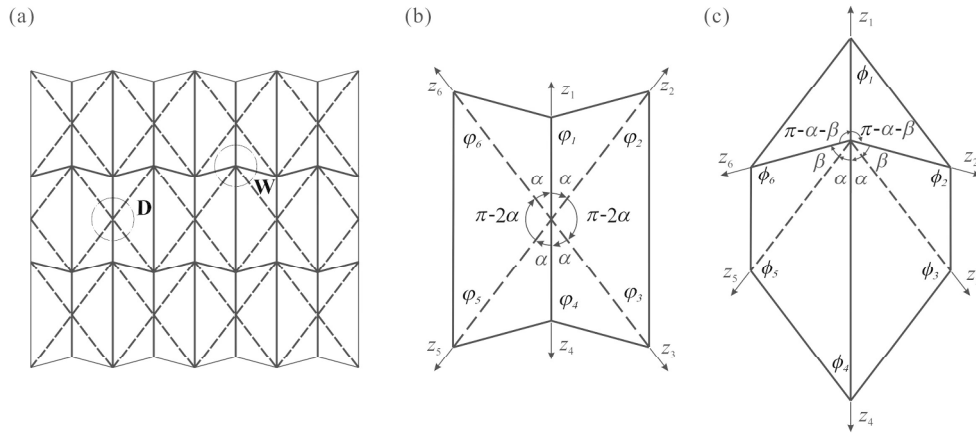
Figure 2   Six-fold waterbomb pattern. (a) The general tessellation of six-fold waterbomb pattern; (b) vertex **D** and its surrounding creases; and (c) vertex **W** and its surrounding creases.
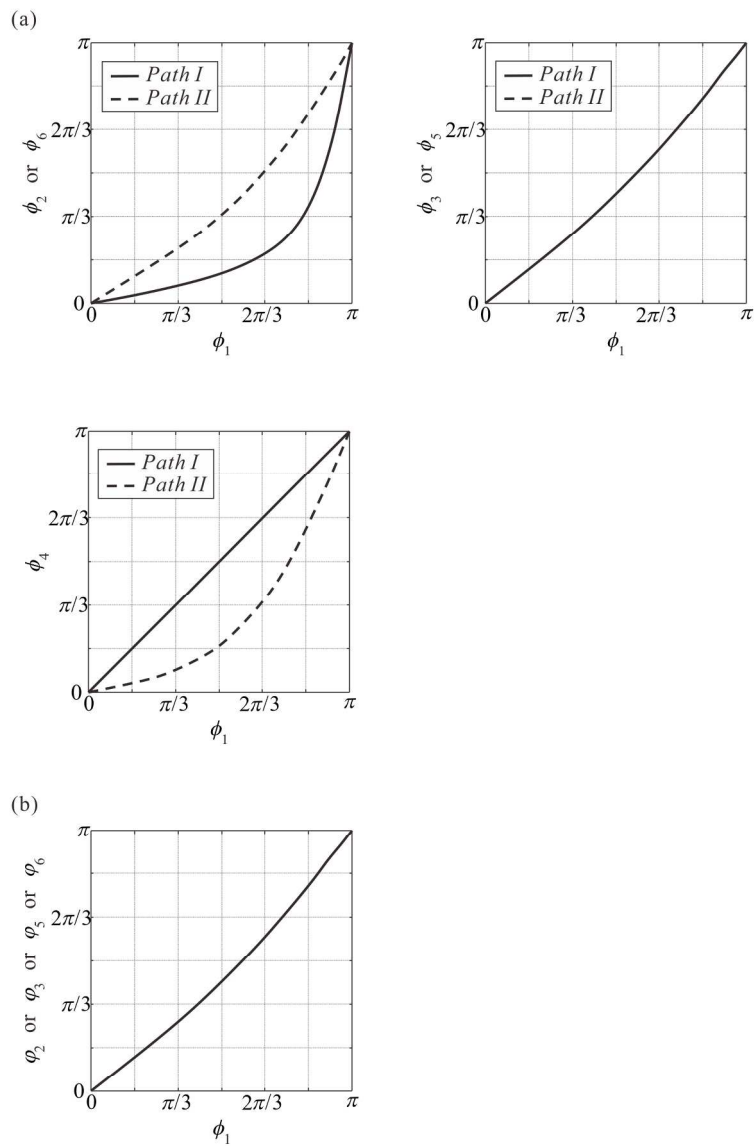
Figure 3   Kinematic behaviour of the waterbomb origami pattern with $\alpha = \dfrac{2\pi}{9}$, $\beta = \dfrac{2\pi}{9}$. Kinematic relationships of vertices (a) **W** and (b) **D**; and (c) two folding paths with configurations i to viii.

Figure 4   Two-stage motion of *Path I* with $\alpha = \dfrac{\pi}{4}$, $\beta = \dfrac{\pi}{4}$. (a) folding paths with configurations i to xi; and (b) kinematic relationships of vertex **W**.

Figure 5   Blockage of waterbomb origami pattern. (a) kinematic curve between ϕ_4 and ϕ_1 of unit **W** with $\alpha = \dfrac{7\pi}{36}$, $\beta = \dfrac{\pi}{4}$; (b) folding manners with $\alpha = \dfrac{7\pi}{36}$, $\beta = \dfrac{\pi}{4}$; (c) folding manners with $\alpha = \dfrac{\pi}{6}$, $\beta = \dfrac{\pi}{3}$, in which the framed configurations are with physical blockage.

Figure 6   Parameter setup for vertices (a) **D** and (b) **W** in thick panels.

Figure 7   Kinematic paths of thick panel waterbomb when $\alpha = \dfrac{7\pi}{36}$, $\beta = \dfrac{\pi}{4}$, $\mu = 0.5$. Kinematic relationships at vertices (a) **W** and (b) **D** with ϕ_1' taken as input, where vertex **W** works as a plane symmetric Bricard linkage while vertex **D** works as a line and plane symmetric Bricard linkage; (c) folding path with configurations i to v; (d) folding sequences of physical models of zero-thickness sheets and thick panels.

Figure 8   Folding path of thick panel waterbomb pattern with $\alpha = \dfrac{\pi}{6}$, $\beta = \dfrac{\pi}{3}$, $\mu = 0.7$, in which the framed configurations are with physical blockage.

Figure 9   Folding path of thick-panel waterbomb pattern with $\alpha = \dfrac{7\pi}{36}$, $\beta = \dfrac{\pi}{4}$ and $\mu = \dfrac{\cos(\alpha + \beta) \cdot \sin\alpha}{\sin\beta} = 0.14$.

23

Figure 10   Folding sequence for patterns with $\alpha = \beta = \dfrac{2\pi}{9}$ and $\mu = 1$. (a) Two folding

paths exist; physical models of zero-thickness sheet (top) and thick panel that fold (b) along *Paths I* and (c) *II*, respectively.

Figure A   Setup of coordinates and kinematic parameters for (a) zero-thickness and (b) thick-panel origami according to the DH notation.

24

Captions of table

Table B.   Kinematic behaviour of the general waterbomb tessellation of zero-thickness
                sheets and thick panels
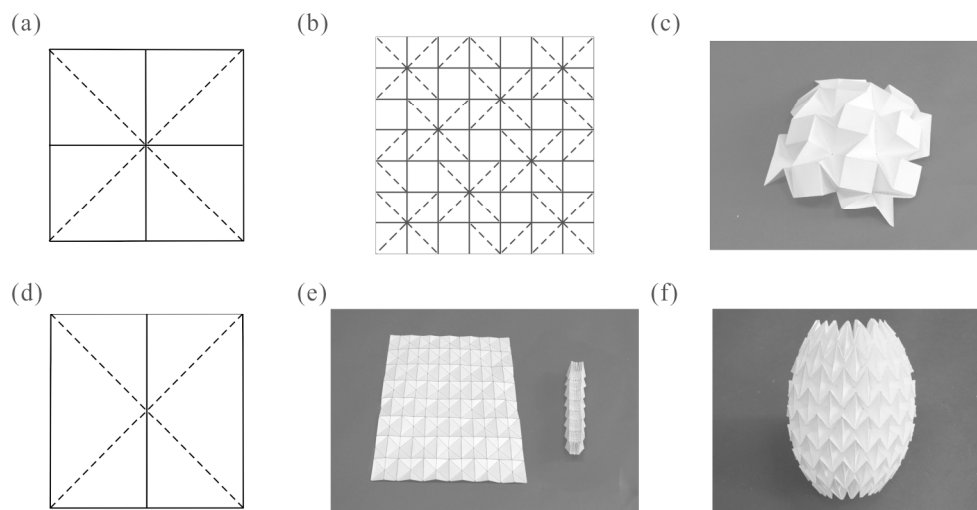
Figure 1. Two waterbomb bases and their tessellations. (a) The eight-fold waterbomb base; (b) One of its tessellations forming the Resch pattern; (c) Partially folded Resch pattern; (d) the six-fold waterbomb base; (e) its tessellation in unfolded and folded states; and (f) the tessellation can also be used to form a tube.
172x90mm (300 x 300 DPI)

1
2
3
4
5
6
7
8
9
10
11
12
13
14
15
16
17
18
19
20
21
22
23
24
25
26
27
28
29
30
31
32
33
34
35
36
37
38
39
40
41
42
43
44
45
46
47
48
49
50
51
52
53
54
55
56
57
58
59
60

(a)　　　　　　　　　　(b)　　　　　　　　　　(c)

Figure 2. Six-fold waterbomb pattern. (a) The general tessellation of six-fold waterbomb pattern; (b) vertex D and its surrounding creases; and (c) vertex W and its surrounding creases.
202x90mm (300 x 300 DPI)

(a)

(b)

Figure 3 Kinematic behaviour of the waterbomb origami pattern with α=β=2π/9. Kinematic relationships of vertices (a) W and (b) D.
168x240mm (300 x 300 DPI)
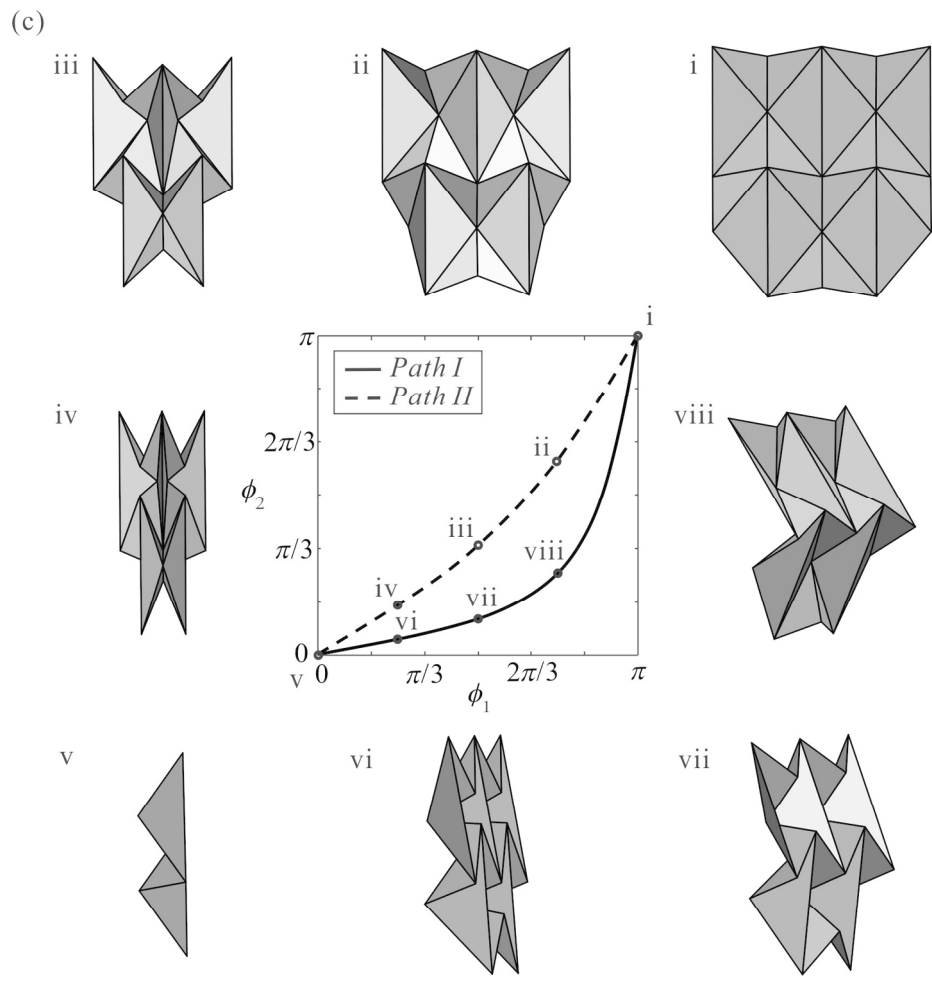
Figure 3 Kinematic behaviour of the waterbomb origami pattern with α=2π/9, β=2π/9. (c) two folding paths with configurations i to viii.
156x160mm (300 x 300 DPI)
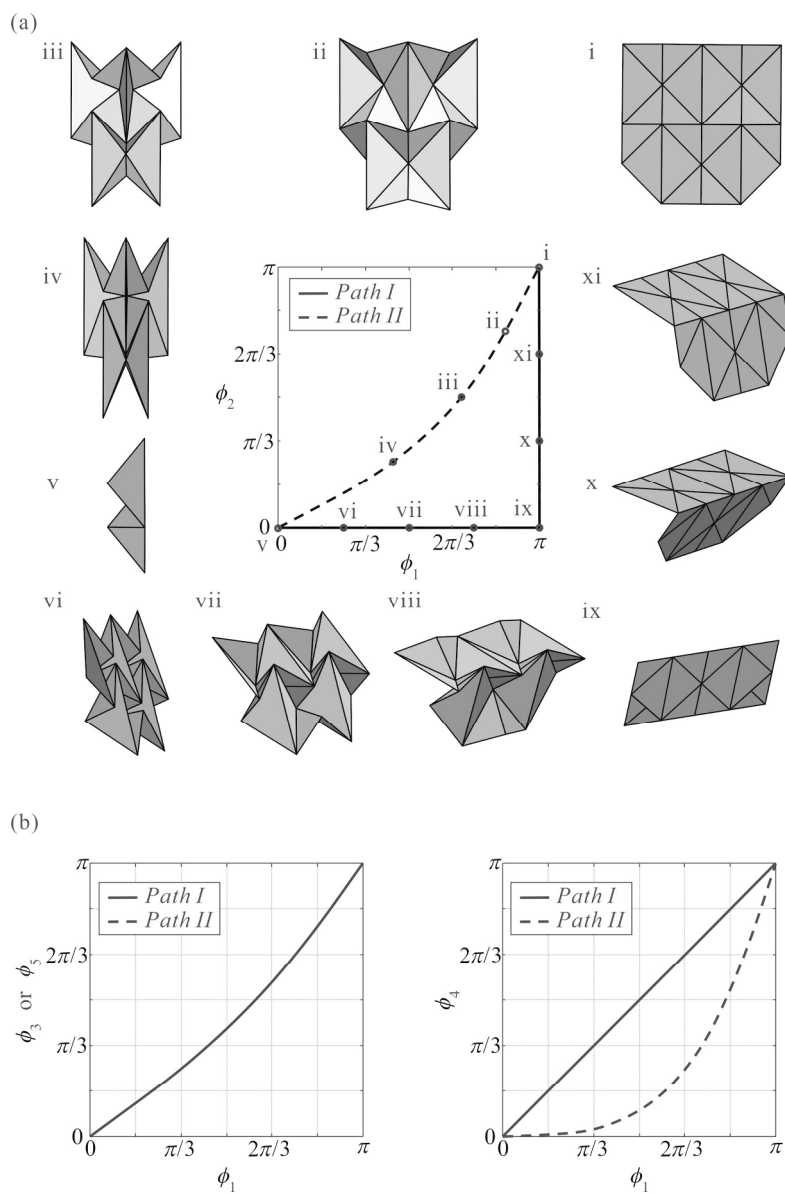
Figure 4 Two-stage motion of Path I with α=π/4, β=π/4. (a) folding paths; and (b) kinematic curves of vertex W.
160x229mm (300 x 300 DPI)
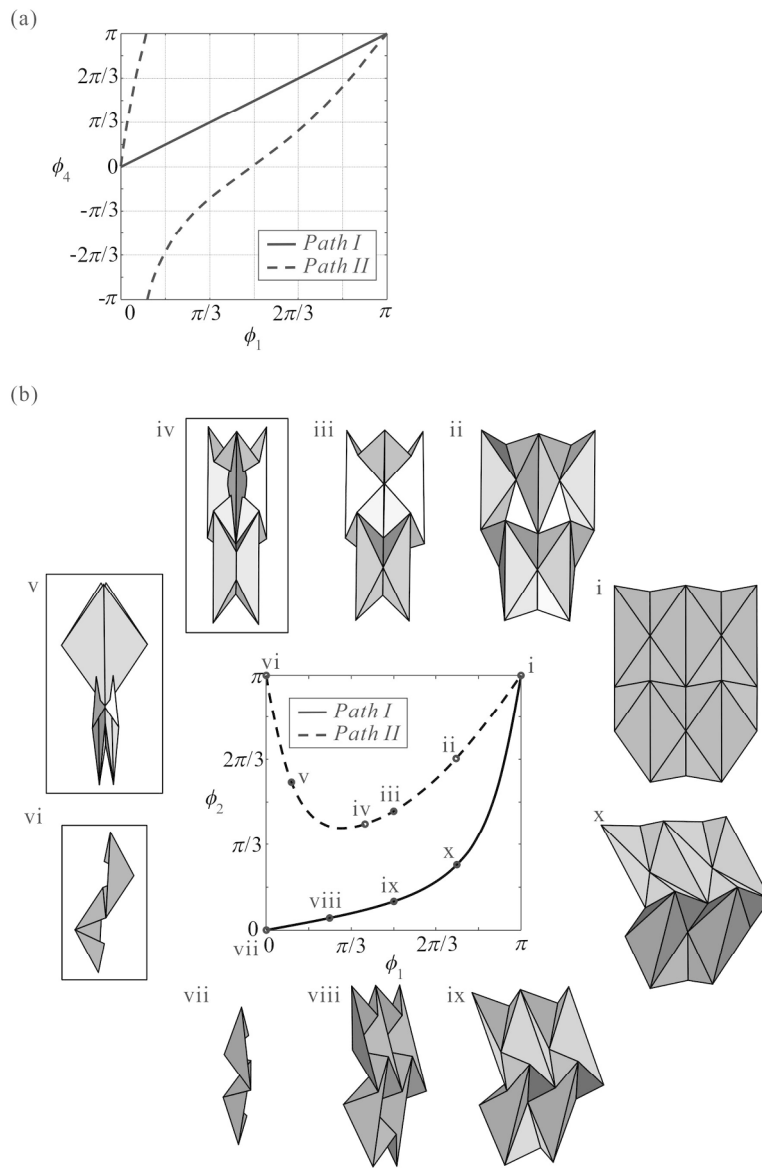
1
2
3
4
5
6
7
8
9
10
11
12
13
14
15
16
17
18
19
20
21
22
23
24
25
26
27
28
29
30
31
32
33
34
35
36
37
38
39
40
41
42
43
44
45
46
47
48
49
50
51
52
53
54
55
56
57
58
59
60

Figure 5. Blockage of waterbomb origami pattern. (a) kinematic curve between   and   of unit W with α=7π/36, β=π/4; (b) folding manners with α=7π/36, β=π/4, in which the framed configurations are with physical blockage.
160x235mm (300 x 300 DPI)
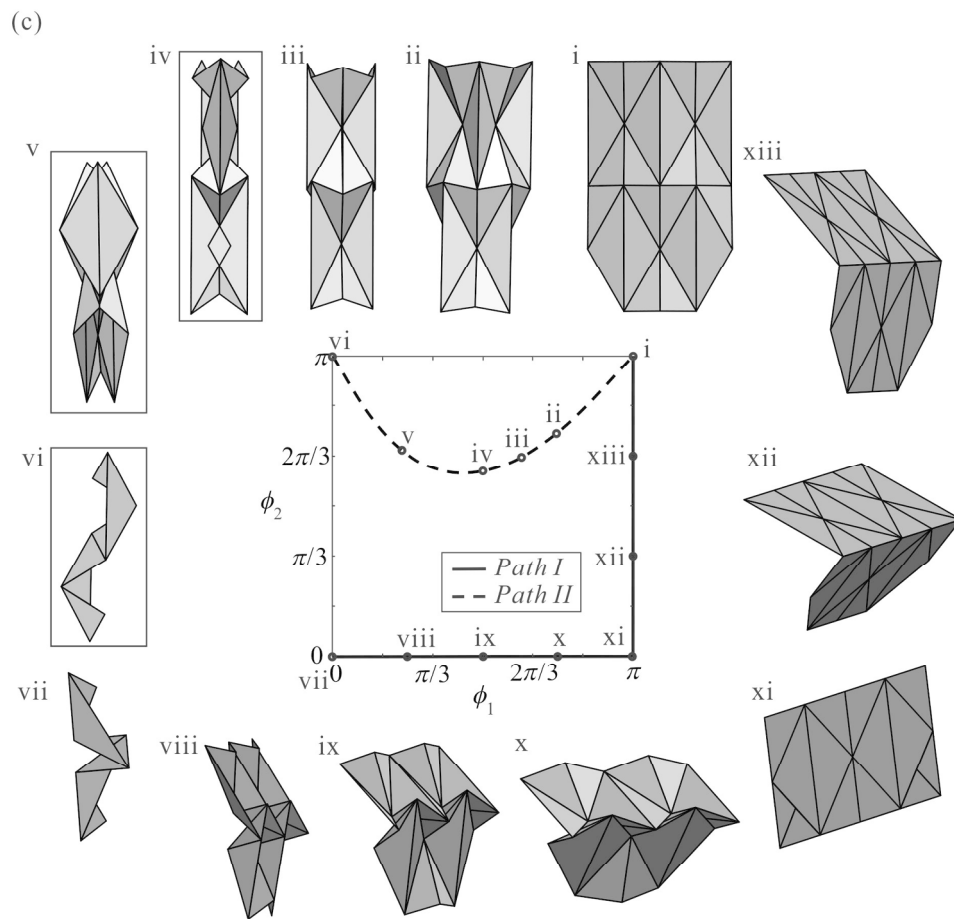
Figure 5. Blockage of waterbomb origami pattern. (c) folding manners with ɑ= п/6, β=п/3, in which the framed configurations are with physical blockage.
166x165mm (300 x 300 DPI)
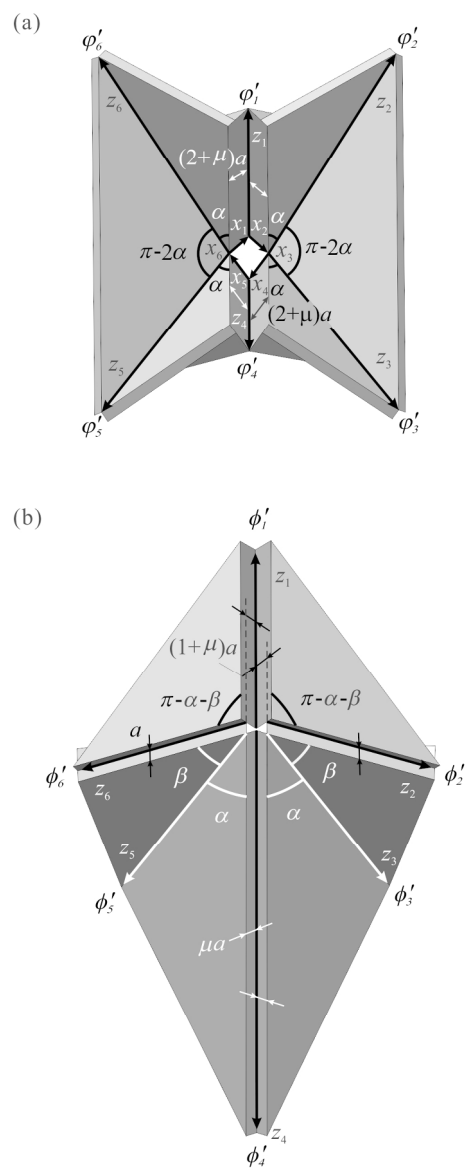
Figure 6. Fold lines around the vertices (a) D and (b) W in thick panels.
104x224mm (300 x 300 DPI)
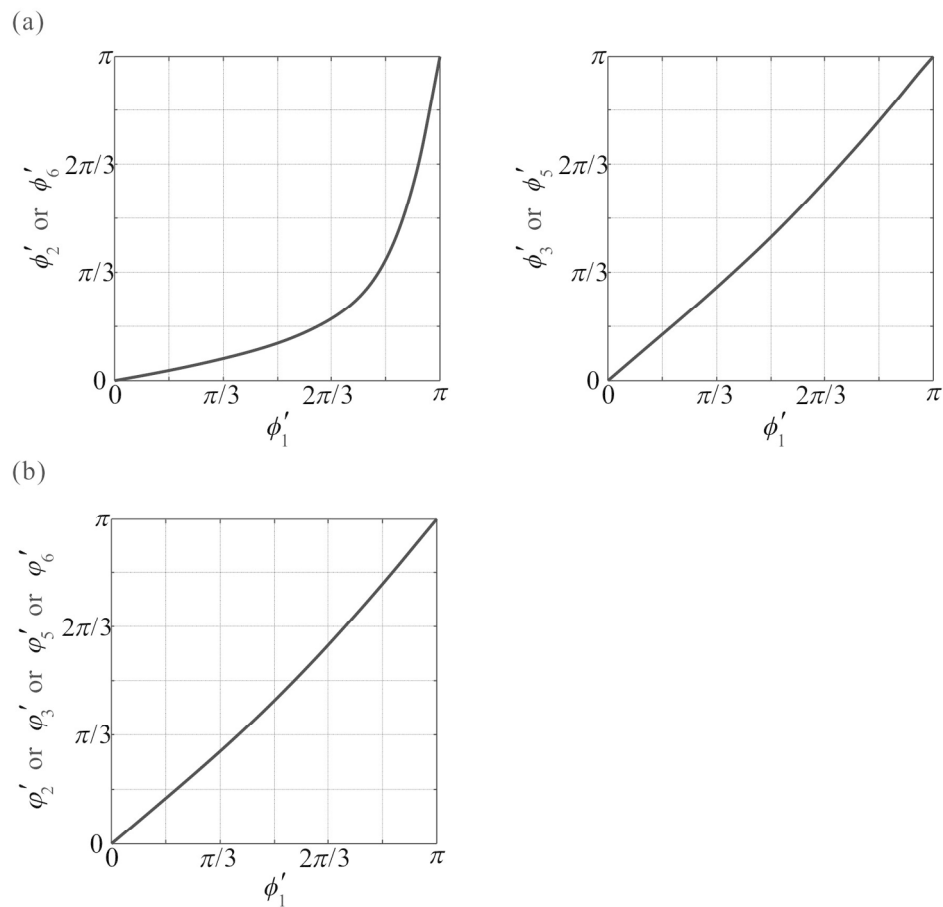
(a)

(b)

Figure 7. The kinematic paths of thick panel waterbomb when ɑ=7π/36, β=π/4, μ=0.5. Kinematic relationships at vertices (a) W and (b) D , where vertex W works as a plane symmetric Bricard linkage while vertex D works as a line and plane symmetric Bricard linkage.
160x150mm (300 x 300 DPI)
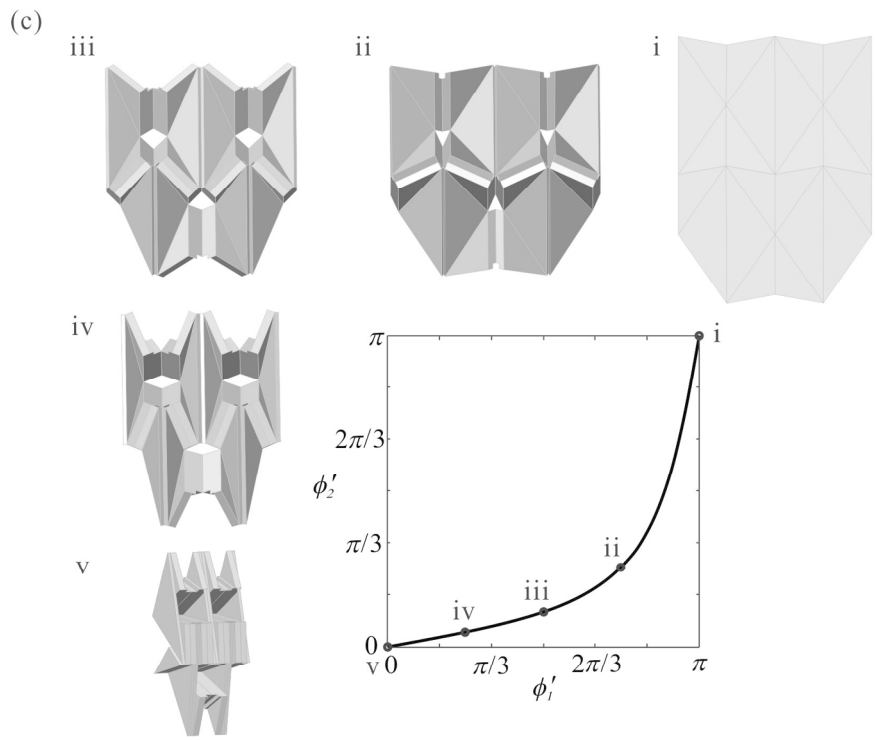
Figure 7. The kinematic paths of thick panel waterbomb when α=7π/36, β=π/4, μ=0.5. Kinematic relationships at vertices (c) folding paths with configurations i to v.
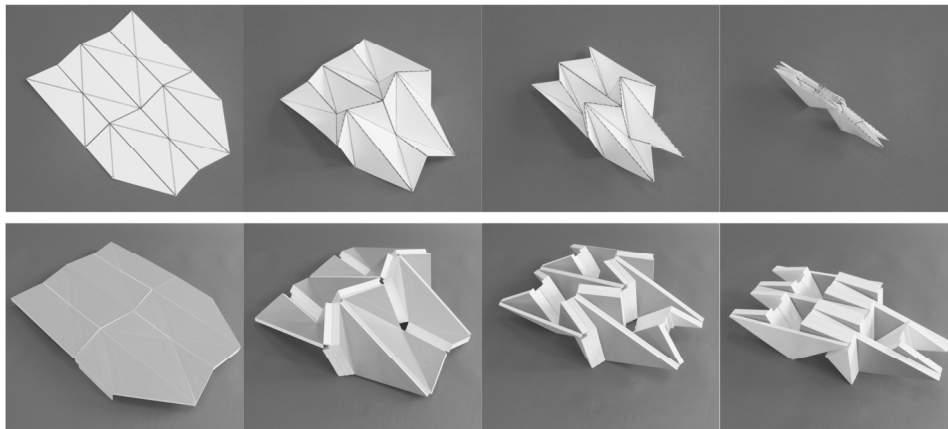160x122mm (300 x 300 DPI)

(d)

Figure 7. The kinematic paths of thick panel waterbomb when α=7π/36, β=π/4, μ=0.5. Kinematic relationships at vertices (d) deployable sequences of models of zero-thickness sheet and thick panel.
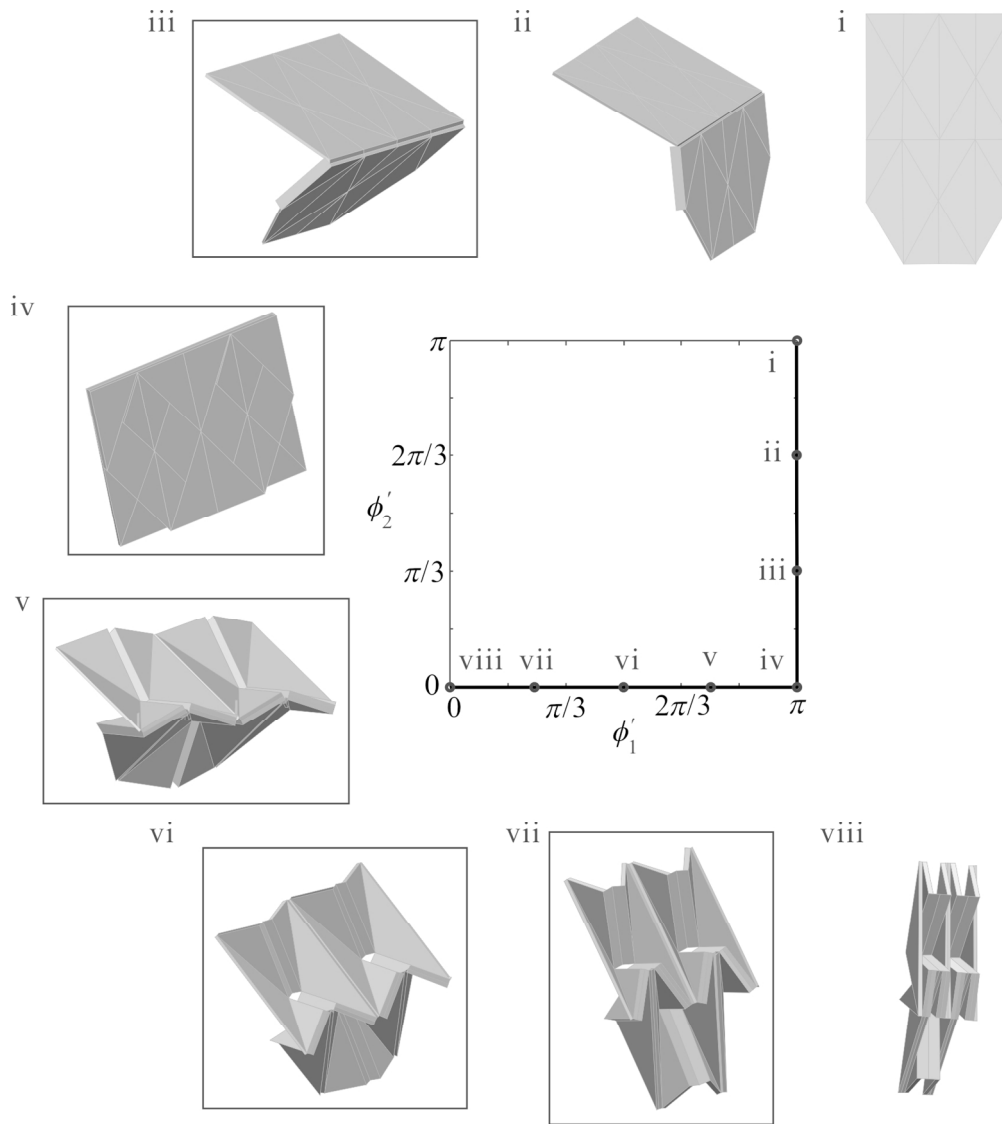168x87mm (300 x 300 DPI)

1
2
3
4
5
6
7
8
9
10
11
12
13
14
15
16
17
18
19
20
21
22
23
24
25
26
27
28
29
30
31
32
33
34
35
36
37
38
39
40
41
42
43
44
45
46
47
48
49
50
51
52
53
54
55
56
57
58
59
60

Figure 8 Folding path of thick panel waterbomb pattern with α=π/6, β=π/3, μ=0.7, in which the framed configurations are with physical blockage.
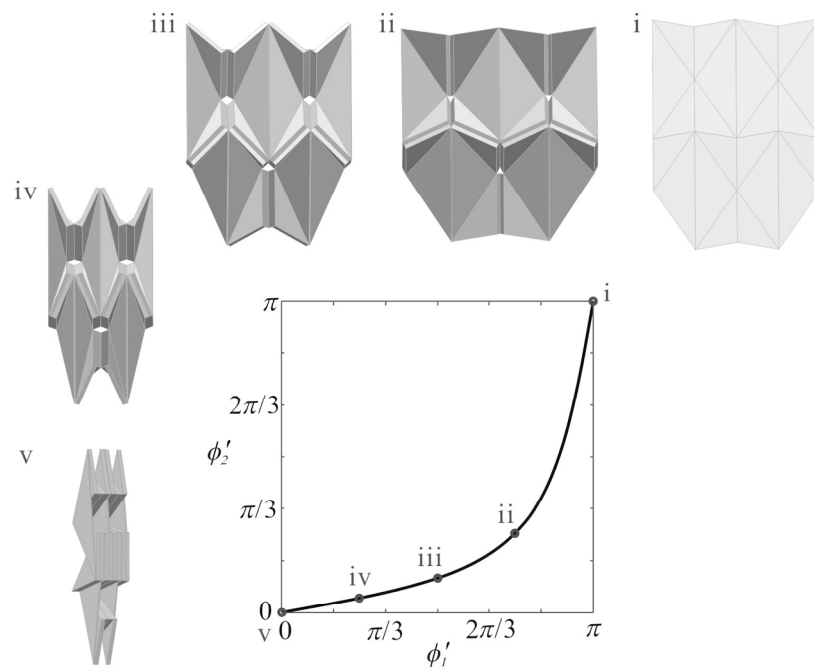144x160mm (300 x 300 DPI)

Figure 9 Folding path of thick panel waterbomb pattern with α=7π/36, β=π/4, μ=0.14.
160x115mm (300 x 300 DPI)

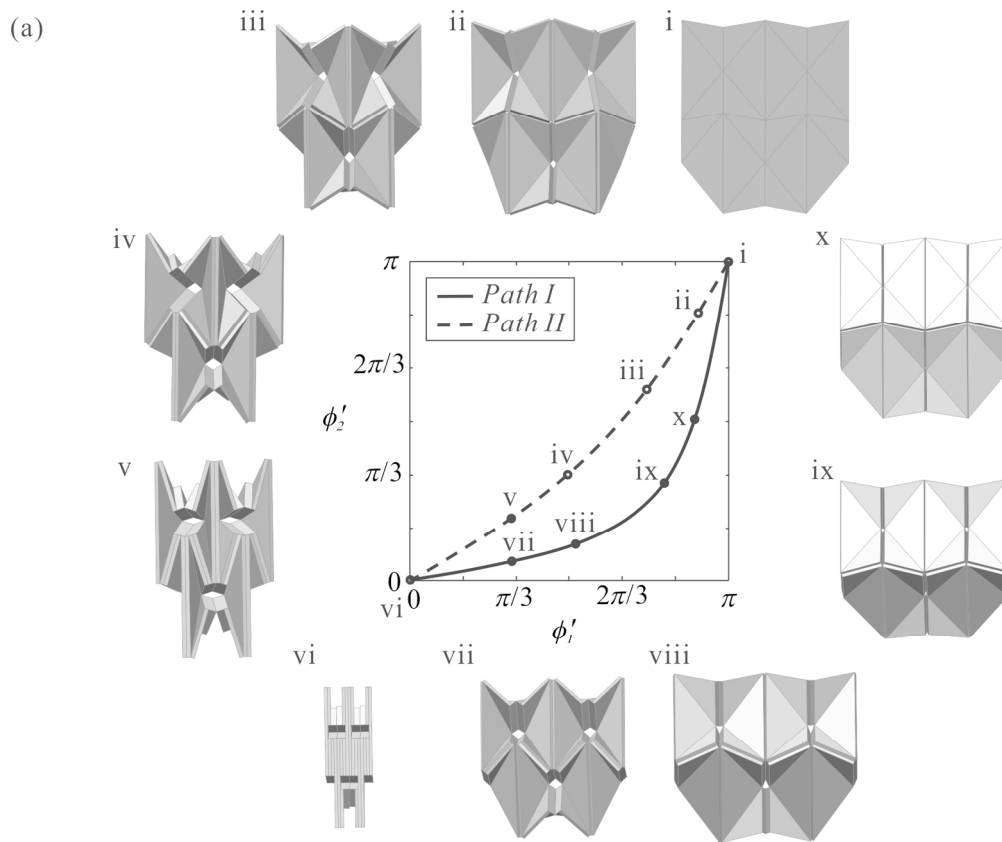Figure 10 Folding sequence for patterns with α=β=2π/9, μ=1. (a) Two folding paths exist.
156x129mm (300 x 300 DPI)

1
2
3
4
5
6
7
8
9
10
11
12
13
14
15
16
17
18
19
20
21
22
23
24
25
26
27
28
29
30
31
32
33
34
35
36
37
38
39
40
41
42
43
44
45
46
47
48
49
50
51
52
53
54
55
56
57
58
59
60

(b)

(c)
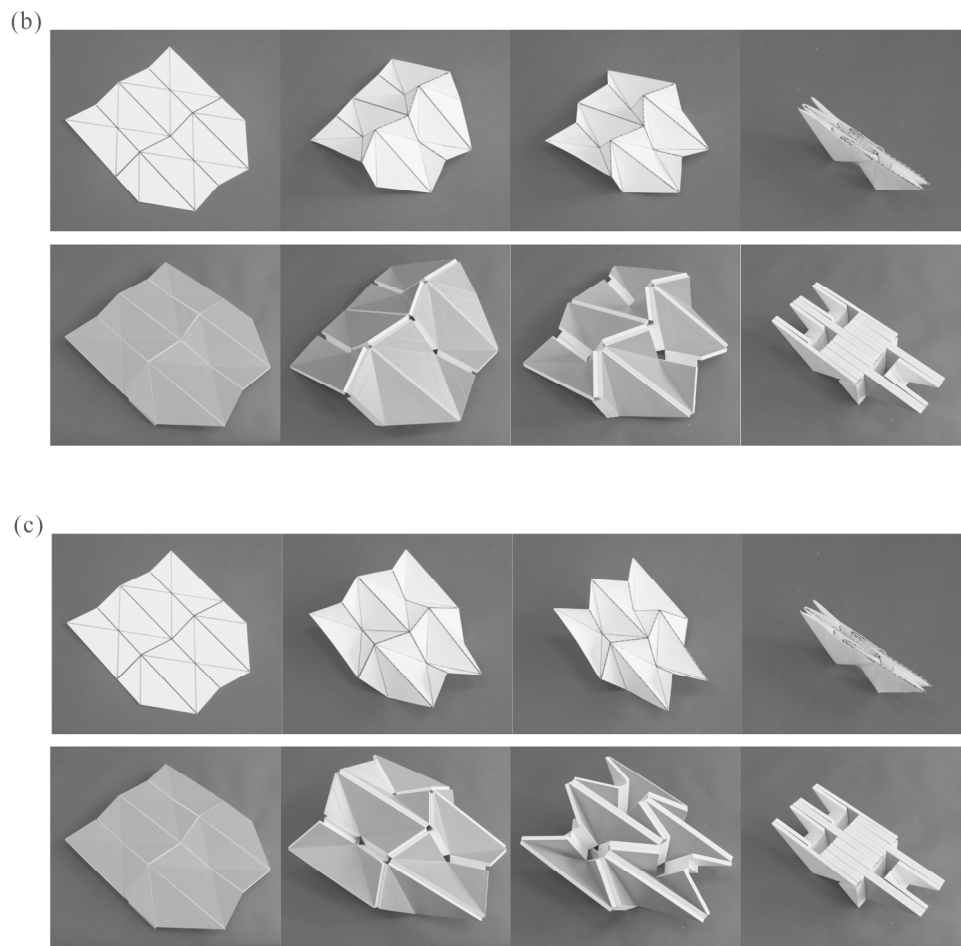

Figure 10 Folding sequence for patterns with α=β=2π/9, μ=1. physical models of zero- thickness sheet (top) and thick panel that fold (b) along Paths I and (c) II, respectively.
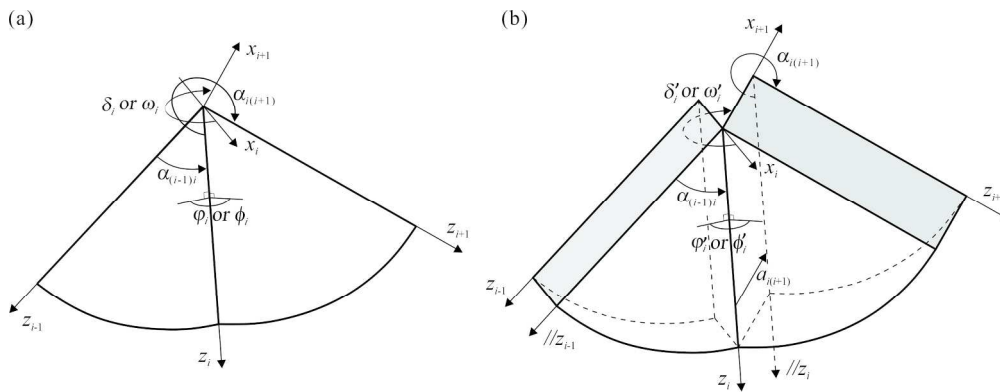173x169mm (300 x 300 DPI)

Figure A Setup of coordinates and kinematic parameters for (a) zero-thickness and (b) thick-panel origami according to the DH notation.
203x77mm (300 x 300 DPI)

Table B. Kinematic behaviour of the general waterbomb tessellation of zero-thickness sheets and thick panels

Geometric conditions		Folding paths	The waterbomb tessellation of zero-thickness sheets	The waterbomb tessellation of thick panels
$\alpha + \beta < \dfrac{\pi}{2}$	$\alpha = \beta$	*Path I*	smooth	smooth
		Path II	smooth	exists only when $\mu = 1$ and the path is smooth
	$\alpha \neq \beta$	*Path I*	smooth	smooth
		Path II	blocked	non-existent
$\alpha + \beta = \dfrac{\pi}{2}$	$\alpha = \beta$	*Path I*	two-stage motion	two-stage motion and blocked
		Path II	smooth	exists only when $\mu = 1$ and the path is smooth
	$\alpha \neq \beta$	*Path I*	two-stage motion	two-stage motion and blocked
		Path II	blocked	non-existent
$\alpha + \beta > \dfrac{\pi}{2}$	$\alpha = \beta$	*Path I*	blocked	blocked
		Path II	blocked while the path for vertex **W** is smooth	exists only when $\mu = 1$ but the path is blocked
	$\alpha \neq \beta$	*Path I*	blocked	blocked
		Path II	blocked	non-existent

1